



Inter-Vesicle Signal Transduction Using a Photo-Responsive Zinc Ionophore

Shaun A. Gartland, Toby G. Johnson, Euan Walkley, and Matthew J. Langton*

Abstract: Transmission of chemical information between cells and across lipid bilayer membranes is of profound significance in many biological processes. The design of synthetic signalling systems is a critical step towards preparing artificial cells with collective behaviour. Here, we report the first example of a synthetic inter-vesicle signalling system, in which diffusible chemical signals trigger transmembrane ion transport in a manner reminiscent of signalling pathways in biology. The system is derived from novel *ortho*-nitrobenzyl and BODIPY photo-caged Zn^{II} transporters, in which cation transport is triggered by photo-decaging with UV or red light, respectively. This decaging reaction can be used to trigger the release of the cationophores from a small population of sender vesicles. This in turn triggers the transport of ions across the membrane of a larger population of receiver vesicles, but not across the sender vesicle membrane, leading to overall inter-vesicle signal transduction and amplification.

Lipid bilayer membranes are essential in nature for cellular compartmentalization. Transmission of chemical information across these membranes and between compartments is a fundamental process for all living organisms. Diffusible signalling molecules form the basis of inter-cellular signalling.^[1] Cell-to-cell communication enables collective behavior, where the function of multiple cells may be coordinated through the sending and receiving of signalling molecules. We and others have developed a range of transmembrane signalling systems in which chemical information is transmitted across a membrane, without mass transport of the chemical signal.^[2] However, inter-vesicle or inter-cell signalling systems employing synthetic components are extremely rare,^[3] and typically biological components are instead utilised to achieve signal transduction.^[4] Regulated transport of small molecules and ions across membranes is itself a form of signal transduction. Significant

effort has been devoted to the development of ionophores, particularly for anions such as chloride, driven by their potential application as therapeutics for channelopathies and cancer, or as tools for chemical biology.^[5] Surprisingly however, transporters for cations, in particular for transition metal elements, remain extremely rare.^[6] Stimuli-responsive transporters, in which ion transport activity can be regulated with an external stimuli, are gathering increasing attention for targeted activation applications,^[7] including photo-switchable,^[8] photo-caged^[9] and redox-responsive^[10] transporters for anions. Burdette and co-workers have reported membrane permeable zinc complexes from which cation release is triggered with light,^[11] but to the best of our knowledge, photo-responsive cation carriers able to catalytically shuttle an excess of ions across a membrane have not been reported.

Herein we report a photo-responsive inter-vesicle signalling system which exploits photo-regulated inter-vesicle diffusion and carrier-mediated transport. Caging the zinc ionophore clioquinol with photo-protecting groups (PPGs) deactivates ion transport, and prevents diffusion of the pro-carrier between vesicles. In situ activation by photo-irradiation leads to its release from a small population of sender vesicles, into which ion transport cannot occur, and triggers transport across the membrane of a larger population of receiver vesicles, leading to amplification of signal.

The general design of the inter-vesicle signalling system is shown in Figure 1a. The input signal (light) is used to trigger the release of the cationophore from a small population of sender vesicles (orange) by cleavage of the photo-cage. The cationophore acts as an inter-vesicle signal, and diffuses to the receiver vesicles present in excess (blue), where it incorporates into the membrane and facilitates transmembrane ion transport. This transport changes the ion concentration inside the vesicle generating a fluorescence response (the output signal). Each signal molecule triggers the transport of many ions in a catalytic process, leading to amplification of the signal.

We hypothesised that a photo-caged cationophore could act as both a diffusible signal and ion transporter, provided that the cage inhibited both transport *and* diffusion between vesicles. Photo-caging is a widely used strategy to suppress activity of biomolecules until reactivated by photo-irradiation,^[12] and has also been used to develop photo-labile chelators.^[13] Photo-caged derivatives of clioquinol were identified as suitable targets, given previous precedence for photo-decaging of quinoline derivatives.^[14] Clioquinol (**1**) is a chelating quinoline-based cationophore which forms neutral 2:1 ligand:metal complexes with Cu²⁺ and

[*] S. A. Gartland, T. G. Johnson, E. Walkley, Prof. M. J. Langton
 Department of Chemistry, University of Oxford, Chemistry Research
 Laboratory
 Mansfield Road, Oxford OX1 3TA (UK)
 E-mail: matthew.langton@chem.ox.ac.uk

© 2023 The Authors. Angewandte Chemie International Edition published by Wiley-VCH GmbH. This is an open access article under the terms of the Creative Commons Attribution License, which permits use, distribution and reproduction in any medium, provided the original work is properly cited.

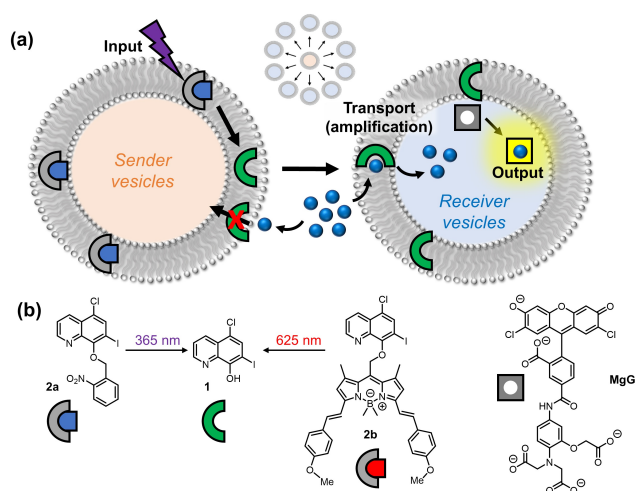


Figure 1. (a) Schematic representation of the inter-vesicle signalling system. The membrane embedded caged-cationophore is released by photo-irradiation from a small population of sender vesicles, and diffuses to a larger population of receiver vesicles. Transmembrane cation transport is triggered by this process only in the receiver vesicles. This process amplifies the signal and generates a fluorescent output. (b) Structures of the zinc transporter **1**, the corresponding photo-caged cationophores **2a** and **2b**, and the zinc ion sensor **MgG**.

Zn^{2+} , and is used as a topical antifungal agent.^[15] It is also known to kill cancer cells, is compatible with liposome-based delivery strategies,^[15d] and has demonstrated membrane transport capabilities.^[6f] Notably, clioquinol also exhibits low micromolar aqueous solubility unlike most lipophilic ionophores, which we anticipated would render it ideal for inter-vesicle signalling.^[16] Blocking of the quinoline phenol O atom with a PPG was expected to lead to two effects. Firstly, to prevent cation binding and hence inhibit transport activity, in line with the mode of action of pro-chelators based on quinoline and other chelating ligands.^[17] Secondly, to enhance the hydrophobicity and inhibit aqueous solubility, such that it would remain embedded in the membrane of the sender vesicles. Consequently, we anticipated that

photo-deprotection would increase hydrophilicity and aqueous solubility enabling diffusion to the receiver vesicles and reveal the bidentate ion binding site to activate ion transport. Zn^{2+} was identified as a suitable transition metal cation for the transport step.

Clioquinol **1** was functionalized with two different PPGs: *ortho*-nitrobenzyl (decaged at 365 nm) and a red-shifted boron dipyrromethane (BODIPY)^[18] derivative which can be decaged in the so called “therapeutic window”, by irradiation with 625 nm light (Figure 1b). The target photo-caged transporter **2a** was accessed via a Mitsunobu reaction of **1** with the corresponding nitrobenzyl alcohol, and **2b** was prepared by alkylation of **1** with the corresponding BODIPY alkyl bromide^[18c] (full synthetic details and characterization are available in the Supporting Information).

The photo-decaging of **2a** and **2b** to generate **1** was initially studied via ^1H NMR spectroscopy. A solution of **2a** in DMSO-d_6 was irradiated with 365 nm light using an LED (1.3 W), and monitored over time (Figure S17 and S18). Under these conditions the PPG was readily cleaved with a half-life of 400 seconds. Similarly, the BODIPY-caged **2b** could be decaged with red light (625 nm, 0.7 W, $t_{1/2}$ = 40 mins, Figure S19 and S20), albeit with longer irradiation times, consistent with the low quantum yield of decaging for red-shifted BODIPY derivatives.^[19]

To explore the Zn^{2+} transport capability of clioquinol and its caged derivatives, a new fluorescence cation transport assay was devised in which the pentapotassium salt of magnesium green (**MgG**, Figure 1b) was encapsulated within large unilamellar vesicles (LUVs).^[20] This membrane impermeable fluorescein-based turn-on fluorophore is a broad-spectrum sensor for a wide range of divalent metal ions. Carrier-mediated Zn^{2+} transport into the vesicle is reported by an increase in **MgG** emission (Figure 2a). The Zn^{2+} transport capabilities of **1**, **2a** and **2b** were determined using this assay with 200 nm 1-palmitoyl-2-oleoyl-*sn*-glycero-3-phosphocholine (POPC) LUVs, (lipid concentration 100 μM), loaded with 50 μM **MgG**, 10 μM ethylenediaminetetraacetic acid (EDTA) and buffered with 10 mM HEPES to pH 7.0 in 100 mM NaCl solution. A 100 μM Zn^{2+} trans-

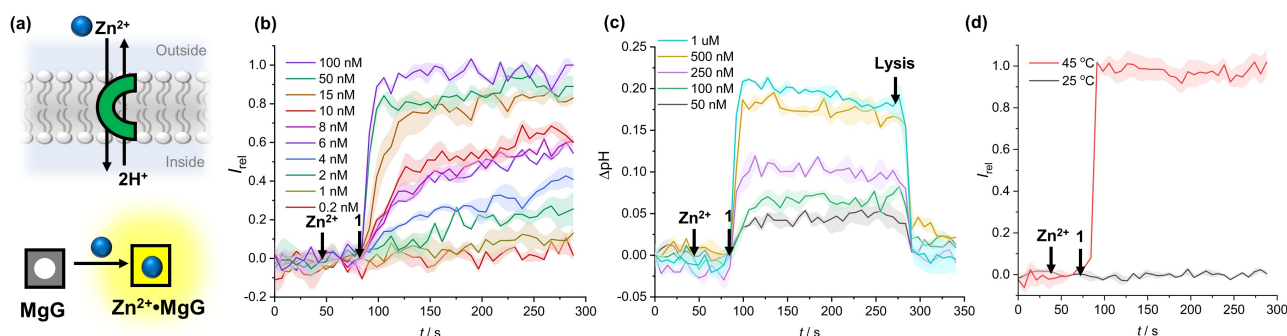


Figure 2. (a) Schematic representation of the $\text{Zn}^{2+}/2\text{H}^{+}$ antiport transport mechanism and detection via **MgG** emission. (b) Change in **MgG** emission, I_{rel} ($\lambda_{\text{ex}} = 506 \text{ nm}$, $\lambda_{\text{em}} = 531 \text{ nm}$) upon addition of **1** in DMSO to POPC LUVs (100 μM) containing 50 μM **MgG**, 100 mM internal and external NaCl, 10 μM internal EDTA and 100 μM external Zn^{2+} , buffered with 10 mM HEPES to pH 7.0. (c) Change in intra-vesicular pH upon addition of **1** in DMSO to a solution containing POPC LUVs (80 μM) containing 1 mM HPTS, with 100 mM internal and external NaCl and 100 μM Zn^{2+} added externally, buffered with 10 mM HEPES to pH 7.0. Lysis with Triton X-100 was used to calibrate the assay by dissipating the pH gradient. (d) Transport in DPPC vesicles in gel (25 $^{\circ}\text{C}$) and fluid (45 $^{\circ}\text{C}$) phases detected via **MgG** emission.

membrane gradient was established by external addition of ZnCl_2 solution. Addition of the carrier (5 μL , DMSO solution), resulted in dissipation of the Zn^{2+} gradient and a concomitant increase in fluorescence emission of **MgG** ($\lambda_{\text{ex}} = 506 \text{ nm}$, $\lambda_{\text{em}} = 531 \text{ nm}$). At the end of each experiment an excess of **1** was added to reach 100 % transport and calibrate the assay. Data for Zn^{2+} transport by **1** is shown in Figure 2b.

Clioquinol **1** proved to be highly active. Hill analysis of the concentration dependence of the activity of **1** was used to determine the effective concentration required to reach 50 % activity (EC_{50}) of $6.7 \pm 0.7 \text{ nM}$ (Figure S19). A Hill coefficient of ≈ 2 is indicative of a 2:1 carrier to ion complex involved in the transport process, consistent with the neutral 2:1 complex observed in previously reported structural studies.^[15a] We hypothesised that the transport mechanism likely involved $\text{Zn}^{2+}/2\text{H}^+$ antiport. The activity of **1** was unchanged upon addition of carbonyl cyanide-*p*-trifluoromethoxyphenylhydrazone (FCCP), a weak acid protonophore at a low concentration (0.8 μM), insufficient to cause activity alone (Figure S22–24). This suggests that, as expected, the transport of the divalent zinc cation is rate limiting.

To further probe the mechanism of ion transport, we adapted the common pH dissipation assay in which, typically, POPC LUVs are loaded with 8-hydroxypyrene-1,3,6-trisulfonate (HPTS, a pH sensitive fluorophore) and the ability of an ionophore to dissipate an applied pH gradient is monitored via changes in the HPTS fluorescence. To explore the postulated coupled $\text{Zn}^{2+}/\text{H}^+$ transport process, we replaced the base pulse with a ZnCl_2 pulse, such that Zn^{2+} transport mediated by **1**, coupled to a proton transport process, is reported by a change in intra-vesicle pH. This is in turn reported by recording the change in the HPTS emission I_{rel} ($\lambda_{\text{em}} = 510 \text{ nm}$) over time following excitation at $\lambda_{\text{ex}} = 405/460 \text{ nm}$ (Figure 2c). An increase in intra-vesicle pH was observed upon addition of **1** in the presence of a 100 μM external Zn^{2+} gradient. The magnitude of this pH change increased with increasing carrier concentration, indicative of carrier-mediated $\text{Zn}^{2+}/2\text{H}^+$ antiport (or the functionally equivalent $\text{Zn}^{2+}/2\text{OH}^-$ symport, which cannot be distinguished). However, given the latter would likely require direct coordination of the highly solvated hydroxide anion to zinc in the transported complex, a $\text{Zn}^{2+}/2\text{H}^+$ antiport mechanism is more plausible, facilitated by the acidic phenol moiety in **1** ($\text{p}K_{\text{a}} = 7.3$).^[6c] Suppression of transport activity of **1** in gel phase dipalmitoylphosphatidylcholine (DPPC) LUVs at 25 °C and restoration of activity in the fluid lipid phase at 45 °C provided evidence for a mobile carrier mechanism, ruling out formation of a membrane-spanning channel structure whose activity would be independent of the lipid phase (Figure 2d).

The photo-activation of Zn^{2+} transport was first studied by ex situ irradiation of the caged transporters **2a** and **2b** (40 μM in DMSO) to generate the free carrier in solution prior to addition to the vesicle suspension (100 nM, Figure 3a and 3b, for **2a** and **2b** respectively). Both caged derivatives **2a** and **2b** were inactive due to blocking of the phenolic Lewis basic donor (grey data). Figure 3a shows the

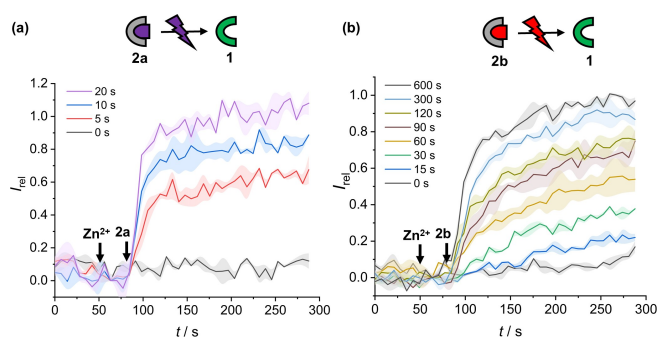


Figure 3. (a) **MgG** zinc transport assay data for **2a** (100 nM), following irradiation with 365 nm light (1.3 W LED) for the specified time prior to the start of the assay and (b) for **2b** (100 nM) following irradiation with 625 nm light (0.7 W LED). Assay conditions as in Figure 2b.

effect of increasing irradiation times on observed transport rate for the *ortho*-nitrobenzyl caged transporter **2a**, in which transport activities comparable to an equivalent concentration of **1** were achieved after 20 seconds of irradiation with 365 nm light in the magnesium green assay. Analogous results for BODIPY-caged **2b** were achieved after 600 seconds of irradiation with red light (625 nm, 0.7 W); indicative of efficient conversion to the decaged carrier under these conditions (Figure 3b). In situ photo-activation, in which **1** is generated from **2a** or **2b** already incorporated into the membrane of LUVs, was achieved by irradiating vesicles containing **2a** or **2b** respectively (Figure S26 and S27). To the best of our knowledge, this represents the first example of a photo-activated cation carrier, and in the case of **2b** notably this is attained using biocompatible red light.

Finally, we explored the possibility of **1** acting as an inter-vesicle signal molecule, via the Scheme shown in Figure 4a, using the *ortho*-nitrobenzyl caged **2a** due to the fast photo-deprotection kinetics. Whilst **1** has reported low micromolar aqueous solubility,^[16] caged-carrier **2a** is sufficiently lipophilic to remain embedded in the membrane of the sender vesicles ($\text{clog}P = 4.9$), confirmed by vesicle leakage experiments using size exclusion chromatography (Figure S36).

To demonstrate inter-vesicle signalling (Figure 4a), two populations of LUVs were prepared. Sender vesicles were generated from DPPC lipids containing pre-incorporated **2a** at 25 °C, but lacking **MgG** in the internal solution. DPPC is in the gel phase below 41 °C and carrier mediated transport is switched off (black data, Figure 2d) which prevents transport of zinc ions into the sender vesicles. The receiver vesicles containing **MgG** were prepared from fluid phase POPC to enable Zn^{2+} transport in the signalling experiment, but without **2a** present. In an initial experiment, the sender and receiver populations of LUVs were mixed in a 1:10 ratio, and compound **2a** was decaged in situ within the membrane of the sender vesicles by irradiating with 365 nm light for 60 s (Figure 4b). Prior to photo-irradiation, no zinc transport in the receiver vesicles was observed. Following photo-decaging of **2a** in the sender vesicles, ion transport was triggered in the receiver vesicles containing **MgG**. A similar signalling process could be achieved even when the

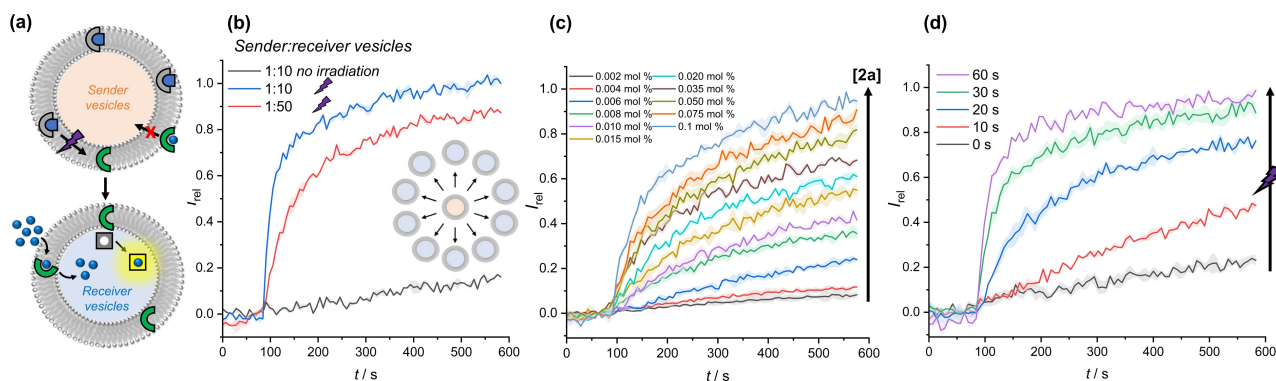


Figure 4. (a) Schematic of the inter-vesicle signalling process between sender vesicles (into which no transport can occur) and a larger population of receiver vesicles. (b) **MgG** assay transport data in POPC receiver vesicles containing **MgG**, following addition of DPPC sender vesicles, containing membrane-embedded **2a** (0.1 mol% with respect to total lipid in the assay) after irradiation with 365 nm light (1.3 W LED) for 60 s. Blue and red data for 1:10 and 1:50 sender: receiver vesicle ratio, respectively. Black data: no irradiation. (c) Dependence of Zn^{2+} transport in receiver vesicles on concentration of **2a** in the sender. (d) Dependence of Zn^{2+} transport in receiver vesicles on irradiation time.

sender vesicles were present in a much lower proportion relative to the receiver (1:50). **1** is considerably more hydrophilic than **2a** in its neutral state ($\log P=3.6$), but the species that diffuses through the aqueous phase is likely to be deprotonated **1** ($pK_a=7.3$),^[6c] which is not possible when alkylated by the PPG. Under the conditions of the experiment in a stirred suspension of vesicles, we estimate the half-life of the combined release, diffusion and membrane uptake process of **1** to be <10 s (Figure S29). Analysis of the dependence of transport rates in the receiver vesicles as a function of **2a** concentration in the sender vesicles revealed an EC_{50} of 14 nM (Figure 4c, Figure S30) which represents the concentration of **2a** released from the sender required to achieve 50 % signal in the receiver population. The extent of Zn^{2+} transport in the receiver could also be directly controlled by varying the irradiation time (Figure 4d), with maximal activity achieved after 60 s of irradiation.

When embedded in the sender vesicles at 0.1 mol% loading with respect to total lipid concentration, photo-decaged **2a** dissipates a 100 μ M transmembrane Zn^{2+} ion gradient in the receiver vesicles. Assuming that once released by photo-irradiation **1** equally distributes between all vesicles in the sample, this corresponds to an amplification of signal of ≈ 600 -fold, i.e. one decaged transporter facilitates the transport of 600 ions before the zinc concentration gradient is equilibrated. In terms of populations of vesicles, this signal transduction and amplification process can be triggered in up to a 50-fold greater population of receiver vesicles. Overall, this therefore equates to an amplification process of up to 30,000 fold with respect to sender vesicles. This is achieved without triggering transmembrane transport of the ion across the sender vesicle membrane, such that the signalling process mediated by transport only occurs in the receiver vesicles.

In conclusion, we report the first examples of photo-responsive Zn^{II} transmembrane ion carriers. These caged clioquinol derivatives include a BODIPY-caged system activated with visible light in the therapeutic window. The

zinc ion transport capabilities of these systems have been studied using a novel fluorescence transport assay utilising vesicle-encapsulated magnesium green, and a zinc-driven pH gradient assay, revealing a Zn^{2+}/H^+ antiport mechanism. Magnesium green has broad cation specificity, so this assay is likely to be broadly applicable to study a wide range of cation transport processes. We have exploited this photo-caged cationophore system to develop an unprecedented synthetic inter-vesicle signalling system, by embedding the caged cationophore within the membrane of sender vesicles with no sensing or transport capabilities. Irradiation of the sender vesicles releases the cationophore, facilitating diffusion of the transporter to a larger population of receiver vesicles, where Zn^{II} transport is initiated. This approach is somewhat reminiscent of a bacterial communication system based on quorum sensing with small diffusible molecules (autoinducers). We anticipate this work will lead to the further study of more complex inter-cellular communication networks, providing new methods to interface artificial and living cells through engineered communication networks, such as between artificial cells and bacterial populations.

Acknowledgements

S. A. G. and M. J. L. acknowledges the Leverhulme Trust (RPG-2020-130) for financial support. T. G. J. thanks the Royal Society and Exeter College, Oxford, for funding. M. J. L. is a Royal Society University Research Fellow.

Conflict of Interest

The authors declare no conflict of interest.

Data Availability Statement

The data that support the findings of this study are available in the supplementary material of this article.

Keywords: Ion Transport • Ionophores • Membranes • Photocaging • Signaling

- [1] G. Krauss, *Biochemistry of Signal Transduction and Regulation*, Wiley, New York, **2006**.
- [2] a) M. J. Langton, F. Keymeulen, M. Ciaccia, N. H. Williams, C. A. Hunter, *Nat. Chem.* **2017**, *9*, 426–430; b) M. J. Langton, N. H. Williams, C. A. Hunter, *J. Am. Chem. Soc.* **2017**, *139*, 6461–6466; c) M. J. Langton, L. M. Scriven, N. H. Williams, C. A. Hunter, *J. Am. Chem. Soc.* **2017**, *139*, 15768–15773; d) P. Barton, C. A. Hunter, T. J. Potter, S. J. Webb, N. H. Williams, *Angew. Chem. Int. Ed.* **2002**, *41*, 3878–3881; e) F. G. A. Lister, B. A. F. Le Bailly, S. J. Webb, J. Clayden, *Nat. Chem.* **2017**, *9*, 420–425; f) K. Bernitzki, M. Maue, T. Schrader, *Chem. Eur. J.* **2012**, *18*, 13412–13417.
- [3] Y. Ding, N. H. Williams, C. A. Hunter, *J. Am. Chem. Soc.* **2019**, *141*, 17847–17853.
- [4] a) P. M. Gardner, K. Winzer, B. G. Davis, *Nat. Chem.* **2009**, *1*, 377–383; b) R. Lentini, S. P. Santero, F. Chizzolini, D. Cecchi, J. Fontana, M. Marchioretto, C. Del Bianco, J. L. Terrell, A. C. Spencer, L. Martini, M. Forlin, M. Assfalg, M. D. Serra, W. E. Bentley, S. S. Mansy, *Nat. Commun.* **2014**, *5*, 4012; c) B. D. Luis, A. Llopis-Lorente, F. Sancenón, R. Martínez-Mañez, *Chem. Soc. Rev.* **2021**, *50*, 8829–8856; d) A. Llopis-Lorente, P. Díez, A. Sánchez, M. D. Marcos, F. Sancenón, P. Martínez-Ruiz, R. Villalonga, R. Martínez-Mañez, *Nat. Commun.* **2017**, *8*, 15511; e) K. P. Adamala, D. A. Martin-Alarcon, K. R. Guthrie-Honea, E. S. Boyden, *Nat. Chem.* **2017**, *9*, 431–439; f) B. C. Buddingh', J. Elzinga, J. C. M. van Hest, *Nat. Commun.* **2020**, *11*, 1652.
- [5] a) J. T. Davis, O. Okunola, R. Quesada, *Chem. Soc. Rev.* **2010**, *39*, 3843–3862; b) S. Matile, A. V. Jentzsch, J. Montenegro, A. Fin, *Chem. Soc. Rev.* **2011**, *40*, 2453–2474; c) J. T. Davis, P. A. Gale, R. Quesada, *Chem. Soc. Rev.* **2020**, *49*, 6056–6086; d) L. E. Bickerton, T. G. Johnson, A. Kerckhoffs, M. J. Langton, *Chem. Sci.* **2021**, *12*, 11252–11274; e) A. V. Jentzsch, S. Matile, in *Anion Transport in Lipid Bilayer Membranes Using Halogen Bonds*, Wiley, Hoboken, **2021**, pp. 195–231.
- [6] a) A. Steinbrueck, A. C. Sedgwick, J. T. Brewster, K.-C. Yan, Y. Shang, D. M. Knoll, G. I. Vargas-Zúñiga, X.-P. He, H. Tian, J. L. Sessler, *Chem. Soc. Rev.* **2020**, *49*, 3726–3747; b) N. Renier, O. Reinaud, I. Jabin, H. Valkenier, *Chem. Commun.* **2020**, *56*, 8206–8209; c) S. M. Kaiser, B. I. Escher, *Environ. Sci. Technol.* **2006**, *40*, 1784–1791; d) D. Magda, P. Lecane, Z. Wang, W. Hu, P. Thiemann, X. Ma, P. K. Dranchak, X. Wang, V. Lynch, W. Wei, V. Csokai, J. G. Hacia, J. L. Sessler, *Cancer Res.* **2008**, *68*, 5318–5325; e) S. Tardito, I. Bassanetti, C. Bignardi, L. Elviri, M. Tegoni, C. Mucchino, O. Bussolati, R. Franchi-Gazzola, L. Marchiò, *J. Am. Chem. Soc.* **2011**, *133*, 6235–6242; f) G. Clergeaud, H. Dabbagh-Bazarbachi, M. Ortiz, J. B. Fernández-Larrea, C. K. O'Sullivan, *Food Chem.* **2016**, *197*, 916–923.
- [7] M. J. Langton, *Nat. Chem. Rev.* **2021**, *5*, 46–61.
- [8] a) A. Kerckhoffs, M. J. Langton, *Chem. Sci.* **2020**, *11*, 6325–6331; b) T. G. Johnson, A. Sadeghi-Kelishadi, M. J. Langton, *J. Am. Chem. Soc.* **2022**, *144*, 10455–10461; c) M. Ahmad, S. Metya, A. Das, P. Talukdar, *Chem. Eur. J.* **2020**, *26*, 8703–8708; d) Y. R. Choi, G. C. Kim, H.-G. Jeon, J. Park, W. Namkung, K.-S. Jeong, *Chem. Commun.* **2014**, *50*, 15305–15308; e) S. J. Wezenberg, L.-J. Chen, J. E. Bos, B. L. Feringa, E. N. W. Howe, X. Wu, M. A. Siegler, P. A. Gale, *J. Am. Chem. Soc.* **2022**, *144*, 331–338.
- [9] a) S. B. Salunke, J. A. Malla, P. Talukdar, *Angew. Chem. Int. Ed.* **2019**, *58*, 5354–5358; b) L. E. Bickerton, M. J. Langton, *Chem. Sci.* **2022**, *13*, 9531–9536.
- [10] a) M. Fares, X. Wu, D. Ramesh, W. Lewis, P. A. Keller, E. N. W. Howe, R. Pérez-Tomás, P. A. Gale, *Angew. Chem. Int. Ed.* **2020**, *59*, 17614–17621; b) B. Zhou, F. P. Gabbai, *Chem. Sci.* **2020**, *11*, 7495–7500; c) G. Park, F. P. Gabbai, *Chem. Sci.* **2020**, *11*, 10107–10112; d) A. Docker, T. G. Johnson, H. Kuhn, Z. Zhang, M. J. Langton, *J. Am. Chem. Soc.* **2023**, *145*, 2661–2668.
- [11] P. N. Basa, C. A. Barr, K. M. Oakley, X. Liang, S. C. Burdette, *J. Am. Chem. Soc.* **2019**, *141*, 12100–12108.
- [12] I. M. Welleman, M. W. H. Hoorens, B. L. Feringa, H. H. Boersma, W. Szymański, *Chem. Sci.* **2020**, *11*, 11672–11691.
- [13] G. C. R. Ellis-Davies, *Chem. Rev.* **2008**, *108*, 1603–1613.
- [14] J. Liu, S. Li, N. A. Aslam, F. Zheng, B. Yang, R. Cheng, N. Wang, S. Rozovsky, P. G. Wang, Q. Wang, L. Wang, *J. Am. Chem. Soc.* **2019**, *141*, 9458–9462.
- [15] a) M. Di Vaira, C. Bazzicalupi, P. Orioli, L. Messori, B. Bruni, P. Zatta, *Inorg. Chem.* **2004**, *43*, 3795–3797; b) P. J. Crouch, M. S. Savva, L. W. Hung, P. S. Donnelly, A. I. Mot, S. J. Parker, M. A. Greenough, I. Volitakis, P. A. Adlard, R. A. Cherny, C. L. Masters, A. I. Bush, K. J. Barnham, A. R. White, *J. Neurochem.* **2011**, *119*, 220–230; c) S. R. Bareggi, U. Cornelli, *CNS Neurosci. Ther.* **2012**, *18*, 41–46; d) M. Wehbe, A. K. Malhotra, M. Anantha, C. Lo, W. H. Dragowska, N. Dos Santos, M. B. Bally, *Drug Delivery Transl. Res.* **2018**, *8*, 239–251.
- [16] R. A. Cherny, C. S. Atwood, M. E. Xilinas, D. N. Gray, W. D. Jones, C. A. McLean, K. J. Barnham, I. Volitakis, F. W. Fraser, Y.-S. Kim, X. Huang, L. E. Goldstein, R. D. Moir, J. T. Lim, K. Beyreuther, H. Zheng, R. E. Tanzi, C. L. Masters, A. I. Bush, *Neuron* **2001**, *30*, 665–676.
- [17] Q. Wang, K. J. Franz, *Acc. Chem. Res.* **2016**, *49*, 2468–2477.
- [18] a) T. Slanina, P. Shrestha, E. Palao, D. Kand, J. A. Peterson, A. S. Dutton, N. Rubinstein, R. Weinstein, A. H. Winter, P. Klán, *J. Am. Chem. Soc.* **2017**, *139*, 15168–15175; b) J. A. Peterson, L. J. Fischer, E. J. Gehrmann, P. Shrestha, D. Yuan, C. S. Wijesooriya, E. A. Smith, A. H. Winter, *J. Org. Chem.* **2020**, *85*, 5712–5717; c) K. Sitkowska, M. F. Hoes, M. M. Lerch, L. N. Lameijer, P. van der Meer, W. Szymański, B. L. Feringa, *Chem. Commun.* **2020**, *56*, 5480–5483; d) J. A. Peterson, C. Wijesooriya, E. J. Gehrmann, K. M. Mahoney, P. P. Goswami, T. R. Albright, A. Syed, A. S. Dutton, E. A. Smith, A. H. Winter, *J. Am. Chem. Soc.* **2018**, *140*, 7343–7346.
- [19] P. Shrestha, A. Mukhopadhyay, K. C. Dissanayake, A. H. Winter, *J. Org. Chem.* **2022**, *87*, 14334–14341.
- [20] M. Liu, X. Yu, M. Li, N. Liao, A. Bi, Y. Jiang, S. Liu, Z. Gong, W. Zeng, *RSC Adv.* **2018**, *8*, 12573–12587.

Manuscript received: June 27, 2023

Accepted manuscript online: July 27, 2023

Version of record online: August 10, 2023